university of groningen

University Medical Center Groningen

University of Groningen

Role of Defects in Tuning the Electronic Properties of Monolayer WS2 Grown by Chemical Vapor Deposition

Yang, Jie; Gordiichuk, Pavlo; Zheliuk, Oleksandr; Lu, Jianming; Herrmann, Andreas; Ye, Jianting

Published in:
Physica status solidi-Rapid research letters

DOI:
10.1002/pssr.201700302

IMPORTANT NOTE: You are advised to consult the publisher's version (publisher's PDF) if you wish to cite from it. Please check the document version below.

Document Version
Final author's version (accepted by publisher, after peer review)

Publication date:
2017

Link to publication in University of Groningen/UMCG research database

Citation for published version (APA):
Yang, J., Gordiichuk, P., Zheliuk, O., Lu, J., Herrmann, A., & Ye, J. (2017). Role of Defects in Tuning the Electronic Properties of Monolayer WS2 Grown by Chemical Vapor Deposition. *Physica status solidi-Rapid research letters*, *11*(10), [1700302]. https://doi.org/10.1002/pssr.201700302

Copyright
Other than for strictly personal use, it is not permitted to download or to forward/distribute the text or part of it without the consent of the author(s) and/or copyright holder(s), unless the work is under an open content license (like Creative Commons).

Take-down policy
If you believe that this document breaches copyright please contact us providing details, and we will remove access to the work immediately and investigate your claim.

Downloaded from the University of Groningen/UMCG research database (Pure): http://www.rug.nl/research/portal. For technical reasons the number of authors shown on this cover page is limited to 10 maximum.

Download date: 25-11-2020

Role of Defects in Tuning the Electronic Properties of Monolayer WS2 Grown by Chemical Vapor Deposition

Jie Yang, Pavlo Gordiichuk, Oleksandr Zheliuk, Jianming Lu, Andreas Herrmann,and Jianting Ye*

Two-dimensional transition metal dichalcogenides have already attracted enormous research interest. To understand the dependence of electronic properties on the quality and defect morphology is vital for synthesizing high quality materials and the realization of functional devices. Here, we demonstrate the mapping of the conductive variations by conducting atomic force microscopy (C-AFM) in the monolayer tungsten disulfide (WS_2) grown by chemical vapor deposition. The electronic properties are strongly affected by the formation of vacancies in monolayer WS_2 during growth, which is also verified by the photoluminescence. This spatial study of defects provides opportunities for optimization of the growth process for enhancing devices performance of TMDs monolayers.

Keywords
chemical vapor deposition, defects, transition metal dichalcogenides, two-dimensional materials, work function, WS_2

* email address: j.ye@rug.nl

In recent years, semiconducting two-dimensional (2D) transition metal dichalcogenides (TMDs), such asMoS_2, $MoSe_2$, WSe_2, and WS_2, have attracted great attention due to their thickness dependant electrical, optical, and mechanical properties such as the indirect-direct band gap transition by isolating monolayers,[1] valley dependant spin configuration with large spin-orbit splitting (especially in the valence band).[2,3] These unique properties offer great opportunities not only for the fundamental research but also for the development of novel devices such as high performance field-effect transistors,[4] light emitting diodes,[5,6] photo-detectors,[7] and spin-valley controllable devices.[8,9]

For applications, growth of large-area, high-quality synthetic monolayers is highly desired. Recently, chemical vapor deposition (CVD) has been demonstrated as the most promising method to grow large area monolayer TMDs with wafer-sized coverage. [10–12] However, intrinsic imperfections in the CVD grown samples are regarded as the major limiting factors in the performance TMD devices. The influence from the defects on the electrical properties is yet to be fully investigated.

Here, we report the experimental detection of local imperfections in CVD-grown WS_2 monolayers and their influence on the electrical properties. The photoluminescence (PL) mapping unveil the spatial variation of optical properties and the non-stoichiometric growth along the edge of as-grown WS_2 monolayers. Meanwhile, by using conductive AFM, the mapping of local conductivity exhibits significant enhancement along the edges of triangular samples, which is consistent with the reduction of Schottky barrier height by carrier doping from the defects.

CVD Growth of the WS_2 Monolayers: Monolayer triangular flakes of WS_2 were synthesized on SiO_2/Si substrates (SiO_2: 285 nm) by chemical vapor deposition (atmospheric pressure). The precursors: powder of WO_3 (50 mg, >99.995%, Sigma Aldrich) and sulfur (200 mg, >99.99%, Sigma Aldrich) were placed in two ceramic boats at the centre and the upstream side of a one-end-sealed quartz tube, respectively. The SiO_2/Si substrates cleaned by acetone and isopropyl alcohol were suspended 2–3mm above the WO_3 powder in a face-down configuration. Prior to synthesis, the tube was purged by Ar flow of 200 sccm for half an hour. The furnace temperature was ramped from room temperature to 750℃ in 40 min. In the meantime, separately, the sulfur boat was heated using a barrel heater to 200 ℃. Main growth is performed by keeping 750℃ for 10 min under the Ar flow of 100 sccm. After the growth, the sample and furnace were cooled down to room temperature naturally.

Due to the dynamics of local vapor environment during the growth, the morphology of as-grown WS_2 flakes varies along the direction of Ar flow. The coverage and size of the monolayers increase from the center area toward both upstream and downstream edges of the substrate. Atomically thin flakes with up to ≈100 μm sharp triangular facet are reproducibly obtained close to the edge of substrates (inset of Figure 1B). Whereas, monolayer flakes with smaller size (≈10μm) and much less density appear in the centre. As shown in Figure 1B, multilayers also grow together with monolayer flakes in the densely populated edge area.

The topographic characteristics and layer thickness determination were performed by using

a scanning probe microscope (VEECO Dimension V) in tapping mode and ambient conditions. The atomic force microscopy (AFM) characterization of the triangle sample shows atomically flat surface with the typical height of 0.8 nm, indicating that the as-grown WS_2 flakes are monolayers, which is consistent with the previous reports.[13]

The Raman characterization of WS_2 monolayers, as shown in Figure 1D, was conducted by a home built micro-Raman system using 532nm laser excitation with a 100x objective (NA=0.7). The frequency difference between E_{2a}^1 (Γ) and A_{1a}(Γ) mode and the predominating 2LA(M) mode are consistent with the characteristics Raman features of monolayer WS_2 on SiO_2/Si substrates.[14]

Optical Inhomogeneity: Besides the Raman peaks, triangular WS_2 monolayers emit strong PL with single peak maxima locating at around 630nm under excitation at λ_{ex}=532 nm, which is consist with the theoretically predicted excitonic excitation $\approx$2 eV in such monolayers.[15] The excitation power was kept constant (0.6mW) for both PL and Raman spectroscopy. The laser spot diameter was estimated to be $\approx$1 μm.

The fluorescence image was captured under a defocused, spatially homogeneous 488nm CW laser beam excitation (5 W). From the optical and fluorescence image of the identical monolayer WS_2 flakes (Figure 2B and C), we notice the ubiquitous feature that the edge of triangular flake shows much brighter PL than that measured for centre part. It worth noting that the PL spectrum also enhances significantly together with a red shift from the enter to the edges (Figure 2 A), indicating inhomogeneity, which might be caused by doping of charged defects such as impurities or vacancies formed in the as-grown WS_2 monolayers.

Conducting AFM: Both fluorescence image and PL spectrum indicate local fluctuation of electronic properties of the as-grown sample. To have further understanding of the material quality, especially its intrinsic doping profile, we performed further microscopic characterization using conductive atomic force microscopy. Since the contact made by using a C-AFM tip is of nanometre size, C-AFM probes the local electrical transport properties of materials with high spatial resolution.

As shown in a typical device (Figure 3A), the electrodes are patterned on top of the triangular monolayer flake by standard e-beam lithography (Raith 150, 30 kV, 30 μm aperture), electronbeam evaporation (Ti/Au: 5/40 nm) and lift off. The electrical properties are studied by measuring the current flowing through one grounded contact pad while biasing through the Pt/Ir conductive tip (typical working function $\approx$5.4 eV) as shown in the schematic of the setup for C-AFM measurements (Bruker Dimension V Conductive Atomic Force Microscope) in Figure 3B.

Compared with the featureless height profile (Figure 3A), the C-AFM mapping (at constant bias of +7V, Figure 3C) clearly exhibits the electrical inhomogeneity of the WS_2 monolayer flake. The local bright regions in the current image correspond to the area with higher conductivity. Strikingly, enhanced conductivity are observed along the edges of the triangular flake as compared to the interiors, showing clear and sharp stripe-like grains parallel to the triangular crystal boundaries. The height profile and distribution of current in the same cross section are extracted along the white lines simultaneously showing the topographical and conductivity, respectively. In spite of the atomically flat morphology throughout the whole flake, the detected current value has two peaks at the edge in contrast to the inner regions with very low current.

The different conductance between the interiors and edges were further investigated by measuring the I–V characteristics by putting C-AFM tip at the edge and interior of the flake,

respectively. The rectification behavior in typical I–V curves (Figure 4A) clearly reveals the Schottky barriers formed between the tip and the WS_2 monolayer. For the metal-semiconductor (M-S) contact operated at room temperatures, when the semiconductor is intrinsic or moderately doped, the thermionic emission dominates the carrier transport across the M-S barrier.[16] Since the as-grown WS_2 monolayers are generally intrinsic, the current of the Schottky contact as a function of applied bias can be given by the thermionic emission-diffusion theory:

$$I = AA^*T^2\exp\left(\frac{-\Phi_b}{k_BT}\right)\left[\exp\left(\frac{qV_b}{nk_BT}\right) - 1\right] \quad (1)$$

where A is the active area of Schottky contact, A^* is the effective Richardson constant,[17] Φ_b is the Schottky barrier height (SBH), k_B is the Boltzmann constant, n is the ideality factor, q is the electron charge, and V_b is the applied bias voltage.

As shown in Figure 4A, using T=300 K in Eq. (1), the black line can describe the I–V characteristics. According to the equation, the Schottky barrier height could be easily extracted from the $\ln I$ versus V.[16] Subsequently, the change of Schottky barrier height at locations with different conductivity can be deduced as

$$\mathrm{In}\frac{I_1}{I_2} \sim -\frac{\Delta\Phi_b}{k_BT} \quad (2)$$

where I_1 and I_2 are the current though the barrier measured at different locations, respectively. Therefore, we determine that the decrease of Schottky barrier height from the interior to the edge of the flake (Figure 4A) is $\approx$0.15 eV.

Discussion: When placing the C-AFM tip in contact with semiconductor, such as the monolayer WS_2, the M-S contact forms Schottky barriers at the interface. The conductivity is quite sensitive to the change of SBH because the thermionic current decreases exponentially with the increase of barrier height.

Theoretically, the height of the Schottky barrier varies for different contact metals (of different work functions) or as a function of the doping level in semiconductors. In our experiment, by keeping the same metal (Pt/Ir) hence constant work function, the change of Schottky barrier height is therefore caused only by different doping levels in different regions of the monolayer. The change of effective barrier height can be related to electron (n) doping of the intrinsic semiconducting WS_2 monolayers.[16] Doping dependant tunnelling effect and imaging force lowering[16] could contribute to this approach, simultaneously causing large leakage current in the reverse bias, which is also consistently shown in Figure 4A. For the CVD grown monolayers, electron doping is usually caused by intrinsic structural defects, such as sulfur vacancies. According to the previous experimental and theoretical studies,[18,19] sulfur monovacancies (V_S), and divacancies (VS_2), with the lowest formation energies, are considered to be the most commonly observed defects in CVD grown TMDs monolayers.

Since CVD growth is sensitive to the dynamics of local chemical environment, the morphology and crystallinity of the as-grown flakes show wide variation across the substrate, which reflects their different growth status. As shown in the optical images of several typical growth stages (Figure 4B), except forthe fully-grown flakes (right bottom panel), the incomplete growth shows morphology with thin center (monolayer) area surrounded by thick edges. Raman spectra measured at different regions (marked by red and blue spots in the up left panel of Figure 4B show that the thick edges are composed by WO_xS_y. This indicates that seeds of WO_xS_y mixtures

form first during the growth, which is followed by the expansion and thinning from centre to edge by further sulfurization. WS_2 monolayers start to appear in the centre of the flake because of the sufficient sulfurization, then the monolayer area extends to the edge, and finally forms complete monolayer flakes with the correct stoichiometry.

Following this growth scenario, due to insufficient sulfurization, sulfur vacancies are expected to show stronger presence at the edge as compared to the centre. This defect distribution has been verified by the Raman and PL measurements. In WS_2 monolayers, the intrinsic center region and defective boundaries creates higher conducting paths along the edge of the flakes. As shown in the C-AFM image, this is consistent with the larger current and the corresponding stripe patterns along the edges of flakes. The doping effect of the vacancies, which causes the reduction of the Schottky barrier, can be sensitively probed by CAFM, revealing the local chemical environment during the growth. Also, the spatial inhomogeneity of PL shows strong correlation with the spatial variation of conductivity, which is consistent with the electron doping caused by the structural defects.[20,21]

In summary, we studied the spatial distribution of defects in the as-grown CVD monolayers of WS_2 and determined its role in optoelectronic properties. The combined characterization of PL, Raman spectroscopy, and local conductivity mapping using conductive AFM is proved as an effect method to unveil the defective area along the edges of triangular flakes. These combined measurements can provide the essential feedbacks to the CVD synthesis for optimizing the electronic properties of TMDs monolayers.

Acknowledgements

This work is supported by ERC consolidator Grant 648855 (Ig-QPD), and the Stichting voor Fundamenteel Onderzoek der Materie (FOM), which is financially supported by the Nederlandse Organisatie voor Wetenschappelijk Onderzoek (NWO).

[1] K. F. Mak, C. Lee, J. Hone, J. Shan, T. F. Heinz, Phys. Rev. Lett. 2010, 105, 136805.
[2] D. Xiao, G. B. Liu, W. X. Feng, X. D. Xu, W. Yao, Phys. Rev. Lett. 2012, 108, 196802.
[3] Z. Y. Zhu, Y. C. Cheng, U. Schwingenschloegl, Phys. Rev. B 2011, 84, 153402.
[4] B. Radisavljevic, A. Radenovic, J. Brivio, V. Giacometti, A. Kis, Nat. Nanotechnol. 2011, 6, 147.
[5] R. S. Sundaram, M. Engel, A. Lombardo, R. Krupke, A. C. Ferrari, P. Avouris, M. Steiner, Nano Lett. 2013, 13, 1416.
[6] Y. J. Zhang, T. Oka, R. Suzuki, J. T. Ye, Y. Iwasa, Science 2014, 344, 725.
[7] O. Lopez-Sanchez, D. Lembke, M. Kayci, A. Radenovic, A. Kis, Nat. Nanotechnol. 2013, 8, 497.
[8] K. F. Mak, K. L. McGill, J. Park, P. L. McEuen, Science 2014, 344, 1489.
[9] K. F. Mak, K. L. He, J. Shan, T. F. Heinz, Nat. Nanotechnol. 2012, 7, 494.
[10] Y. M. Rong, Y. Fan, A. L. Koh, A. W. Robertson, K. He, S. S. Wang, H. J. Tan, R. Sinclair, J. H. Warner, Nanoscale 2014, 6, 12096.
[11] S. J. Yun, S. H. Chae, H. Kim, J. C. Park, J.-H. Park, G. H. Han, J. S. Lee, S. M. Kim, H. M. Oh, J. Seok, M. S. Jeong, K. K. Kim, Y. H. Lee, ACS Nano 2015, 9, 5510.
[12] Y. H. Lee, L. L. Yu, H. Wang, W. J. Fang, X. Ling, Y. M. Shi, C. T. Lin, J. K. Huang, M. T. Chang, C. S. Chang, M. Dresselhaus, T. Palacios, L. J. Li, J. Kong, Nano Lett. 2013, 13, 3.
[13] H. R. Gutierrez, N. Perea-Lopez, A. L. Elias, A. Berkdemir, B. Wang, R. Lv, F. Lopez-Urias, V. H. Crespi, H. Terrones, M. Terrones, Nano Lett. 2013, 13, 3447.

[14] A. Berkdemir, H. R. Gutierrez, A. R. Botello-Mendez, N. Perea-Lopez, A. L. Elias, C. I. Chia, B. Wang, V. H. Crespi, F. Lopez-Urias, J. C. Charlier, H. Terrones, M. Terrones, Sci. Rep. 2013, 3, 1755.
[15] Y. D. Ma, Y. Dai, M. Guo, C. W. Niu, J. B. Lu, B. B. Huang, Phys. Chem. Chem. Phys. 2011, 13, 15546.
[16] S. M. Sze, K. K. Ng, Physics of Semiconductor Devices, John Wiley & Sons, Hoboken, NJ 2006, chap. 3.
[17] H. L. Shi, H. Pan, Y. W. Zhang, B. I. Yakobson, Phys. Rev. B 2013, 87, 155304.
[18] J. Kunstmann, T. B. Wendumu, G. Seifert, Phys. Status Solidi B 2016, 254, 1600645.
[19] X. Liu, I. Balla, H. Bergeron, M. C. Hersam, J. Phys. Chem. C 2016, 120, 20798.
[20] C. X. Cong, J. Z. Shang, X. Wu, B. C. Cao, N. Peimyoo, C. Qiu, L. T. Sun, T. Yu, Adv. Opt. Mater. 2014, 2, 131.
[21] N. Peimyoo, J. Z. Shang, C. X. Cong, X. N. Shen, X. Y. Wu, E. K. L. Yeow, T. Yu, ACS Nano 2013, 7, 10985.

Figures and Captions

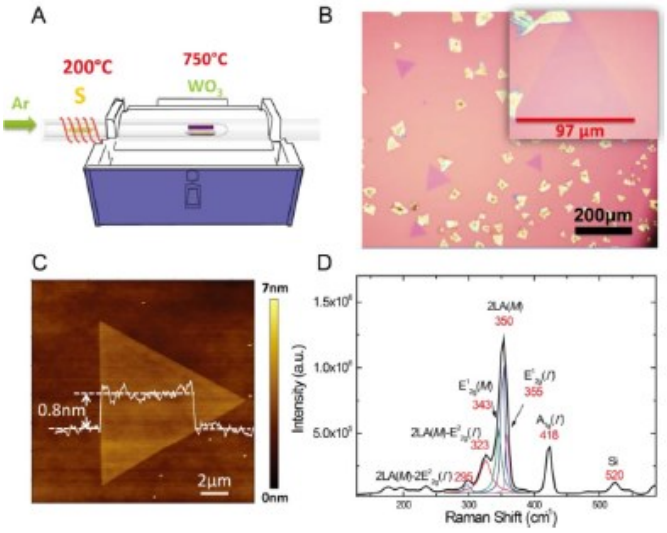

Figure 1. Growth and characterization of monolayer WS_2. (A) Schematic presentation of the CVD system. (B) A large area ($\approx$1x1 mm^2) optical microscopy of WS_2 flakes deposited on the substrate. (C) AFM image of an as-grown WS_2 crystal with the cross-section height profile of the sample as inset. Scale bar: 2µm. The thickness of these thin triangular crystals is determined by the height profile of AFM to be 0.8 nm, which is in agreement with that of reported monolayer WS_2 flakes. (D) Multipeak Lorentzian fitting of Raman spectra in WS_2 monolayer at room temperature.

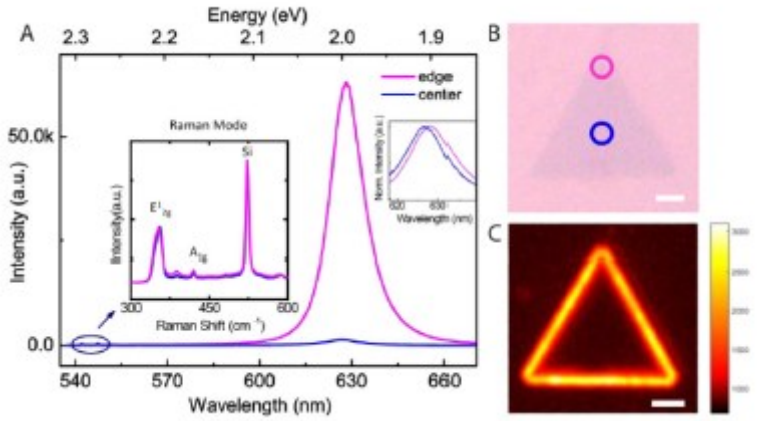

Figure 2. (A) Room-temperature photoluminescence spectra at the different positions, which are indicated by circles of different colors, in the as-grown WS_2 flake shown in the optical image of (B), zoom of the Raman peaks and normalized PL peaks are shown in the inset. PL intensity at the edge is 129 times stronger than that of the centre, while showing a redshift of 1 nm. (B) and (C) optical and fluorescence images of the same 1L-WS_2 triangular flake, scale bar: 2 µm.

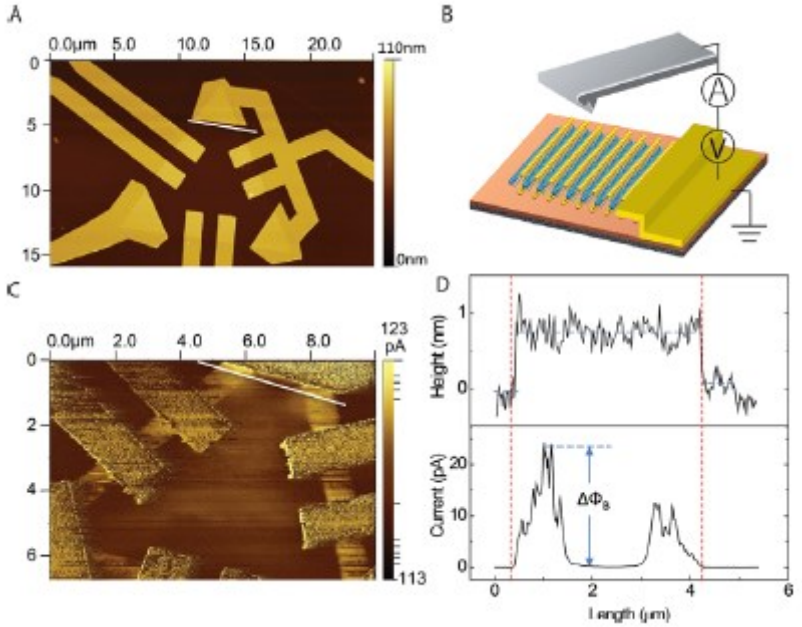

Figure 3. Significant edge-enhancement of conductivity in the monolayer WS_2 flakes. Tapping-mode AFM topographic image (A) and the corresponding current image (C) of the as-grown WS_2 monolayer acquired by C- AFM. Images shown in panel (A) and (C) aremeasured by the same Pt/Ir tip in tapping and TUNA mode, respectively. (B) Schematic diagram of electrical measurement by conductive AFM. (D) Height and current profile from cross section as indicated by the white line in (A) and (C).

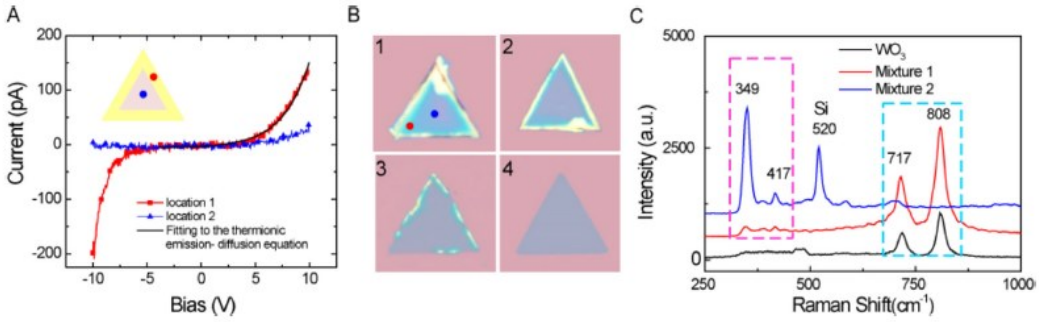

Figure 4. (A) I–V sweeps with both positive and negative bias voltage from -10 to 10 V on the C-AFM contact point corresponding to different locations. The black line is the fitting of the I–V curve using the thermionic emission- diffusion theory. (B) Optical images of WS_2 flakes at different growth stages. (C) Raman spectra measured at the multilayer area and the edge of the flake (as indicated by the red and blue dots in panel B, picture 1). The black spectrum shows the Raman features of pure WO_3 measured from the precursors used in our growth.